Automation in Construction 19 (2010) 875–883

Contents lists available at ScienceDirect

Automation in Construction

journal homepage: www.elsevier.com/locate/autcon

A morphological approach to pipe image interpretation based on segmentation by support vector machine

John Mashford *, Mike Rahilly, Paul Davis, Stewart Burn

Commonwealth Scientific and Industrial Research Organisation, PO Box 56, Highett, Vic. 3190, Australia

ARTICLE INFO

Article history:
Accepted 7 June 2010

Keywords:
Automatic pipe inspection
Colour image segmentation
Support vector machine
Mathematical morphology

ABSTRACT

This paper presents a new approach to automatic pipe inspection using pixel-based segmentation of colour images by support vector machine (SVM) coupled with morphological analysis of the principal connected component of the segmented image. The pixel-based segmentation method has been tested using RGB, HSB, Gabor and local window feature sets and is seen to work best with the HSB feature set. The morphological analysis allows the principal connected component of the segmented image to be decomposed into the pipe flow line region, the pipe joints and adjoining defects. Generalisations of the morphological operations of erosion and dilation are defined and some simple properties of them are derived. A fuzzy approach to pipe connection detection is also described.

1. Introduction

In this paper we propose an approach to signal interpretation for automatic pipe inspection based on colour images. Automatic pipe inspection involves the automatic processing of pipe image or signal data in order to find and classify defects or features and to produce a report about the condition of the pipe. The information obtained from pipe inspection is used to determine if and when maintenance should be carried out for the pipe. We will consider in particular the case of sewer pipe inspection, though the techniques are more generally applicable.

The standard method of inspection of sewer pipes which are not large enough to walk through is to have operators view CCTV signals obtained by inspection devices sent into the pipes. This method is time consuming, error prone and subjective. Even experienced operators may differ considerably in their assessment of the same sewer. Automatic sewer pipe inspection has the potential to avoid these problems.

An early semi-automatic inspection system was the KARO system [1] which consisted of a multi-sensor inspection device and a two pass interpretation system. During the largely automatic first pass a hierarchical fuzzy logic sensor fusion algorithm was used to identify candidate defects which were then investigated in detail by the operator during a second pass.

The PIRAT system [2] was made up of an inspection device providing range images (in which the pixel values are distances) together with an interpretation system using neural networks and other AI techniques [3]. Neural networks have been used in a number of other interpretation systems for automatic pipe inspection [4–6].

Our recent work has focussed on the development of an interpretation system rather than on the building of an inspection device. Data for such an interpretation system could be provided by a commercial inspection system. Such an inspection system will move through a pipe and obtain a number of colour images. We also assume that there is the capability to combine together all of these images to form an unwrapped pipe image. An unwrapped pipe image is an image of the pipe represented in cylindrical polar coordinates. Fig. 1 shows part of such an image. In the present paper we will assume that the interpretation system has access to such an unwrapped pipe image. If this were not the case then it would be necessary either to construct an unwrapped pipe image from the underlying images and then process that or to process each of the individual underlying images and then to weave together all of the processing outputs to form an overall pipe condition report.

The colour images provide significantly different information from grey-scale images or range images. This can augment the effectiveness of some of the image processing tasks that are to be carried out on the images. However, in some other respects, the tasks are more difficult. With colour images, where the information available is that of colour and intensity, there may be no way of determining whether a defect or feature is an intrusion or an extrusion. This is because a patch of pipe surface looks essentially the same if it is translated in space. This means that it may be difficult to distinguish between categories such as “corrosion” and “deposit” for defects. On the other hand it may be that corrosions tend to have a particular colour or texture signature while deposits have another in which case the colour image data would be sufficient to distinguish between them.

With range images it can be determined whether a defect or feature is an intrusion or an extrusion by simply comparing the range values on

* Corresponding author. Tel.: +61 3 9252 6115; fax: +61 3 9252 6253.
E-mail addresses: John.Mashford@csiro.au (J. Mashford), Mike.Rahilly@csiro.au (M. Rahilly), Paul.Davis@csiro.au (P. Davis), Stewart.Burn@csiro.au (S. Burn).

0926-5805/$ – see front matter.
doi:10.1016/j.autcon.2010.06.001

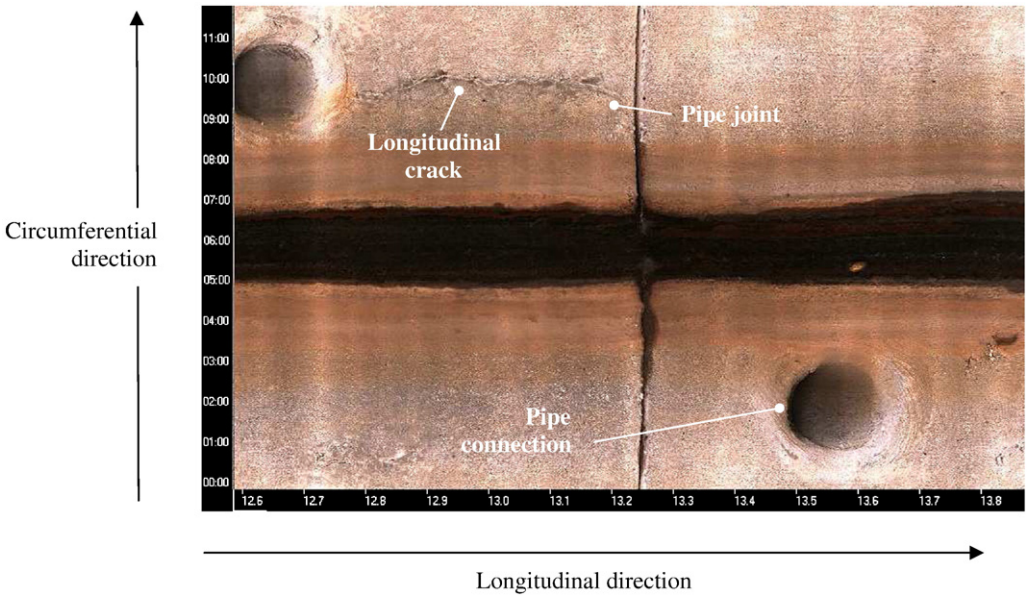

Fig. 1. A section of an unwrapped pipe image.

the defect with the nearby range values off the defect. For this reason we may also assume, when discussing properties related to range values of defects, that the interpretation system has an available unwrapped pipe range image. This range image may be provided by the inspection system or else possibly constructed by processing the colour images obtained by the inspection system using photogrammetry. If photogrammetry is used then the cost of an inspection device would only be the cost of a colour image acquisition system such as in a commercially available system. If the range image is to be obtained from the inspection device then the range image acquisition hardware can be easily integrated, at low cost, into existing camera-based inspection systems [6].

2. The proposed system

The proposed system is based on the PIRAT interpretation system. It consists of pre-processing, segmentation, classification, image analysis and high level system modules. Pre-processing carries out such operations as smoothing and filtering to put the pipe image in a suitable form for the subsequent processing modules. The segmentation module partitions the input image into meaningful subsets. In the case of two class segmentation each subset is either a "region of interest" (ROI) or "good pipe". Segmentation can be effected by pixel labelling combined with connected component labelling. The image classification module classifies each ROI output by segmentation as being in one of a number of classes such as "hole", "corrosion", "pipe connection", "deposit" and "tree root".

A basic difference between the proposed system and the PIRAT system is that the segmentation operates using colour digital images rather than range images. This opens up the possibility of more effective segmentation using colour information. A schematic diagram for the proposed system is given in Fig. 2.

A major difference resulting from using colour image data is that it is difficult to generate suitable simulated data. This means that the pixel labelling classifier for segmentation and the image classifier have to be trained from real data. If neural networks or related classifiers are used then these classifiers require hundreds or thousands of training cases for training. For the case of the pixel labeller this may not be so bad because just one image contains many thousands of pixels.

However, for training the image classifier many hundreds of images would be required. This is unlikely to be feasible. Therefore the proposed system will not use image classification by neural network or similar classifier as in the PIRAT system. Rather image classification can be carried out as part of image analysis or by using multiclass segmentation.

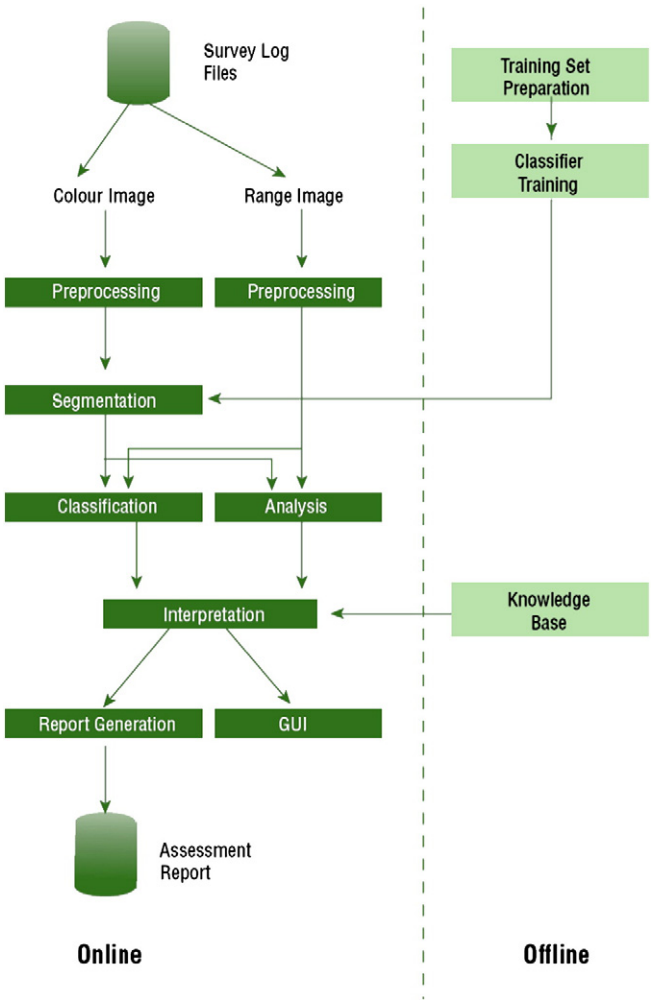

Fig. 2. Schematic diagram of proposed system.

A decision tree classifier can be implemented in a similar fashion to the implementation of the classifier that was used in the PIRAT system. The fundamental decision that has to be made about an ROI is whether it is an intrusion or an extrusion. This can be made by comparing the average range value of on-defect pixels with the average range value of off-defect pixels which are in a neighbourhood of the boundary of the defect.

The difference of these values in the case when the defect is determined to be an extrusion can be used to assign the defect to being either a hole or a corrosion. Alternatively, by using appropriate fuzzy membership functions, the defect can be assigned fuzzy membership function values in the classes "hole" and "corrosion".

Some holes can be identified as pipe connections by means of a pipe connection detector which examines the dimensions and location of the defect and may compute the ellipse of best fit for the boundary of the defect in order to give a compound fuzzy membership value.

Intrusive defects can be given a deterministic or fuzzy classification as either tree roots or deposits by use of a tree root detector which computes the maximum deviation between the range values of off-defect pixels and on-defect pixels in windows centred on boundary points of the defect.

Thus it is possible to construct a deterministic or fuzzy image classification module for the problem without using neural network classifiers. In fact the PIRAT system image classifier which performed best out of all the versions tried was constructed largely on this basis as a decision tree utilising, for the most part, simple detectors. The most effective of the neural network classifier based detectors was the pipe connection/hole classifier which can be implemented just as effectively without using neural networks in the manner described above.

3. The segmentation sub-system

There are a number of approaches to colour image segmentation including thresholding, feature based clustering, region-based approaches, edge detection approaches, fuzzy approaches and neural network approaches [7].

The simplest approach is to threshold the brightness and then to carry out connected component labelling. This has been carried out in the system of Moselhi and Shehab-Eldeen [8]. The resulting segmentation is dependent upon the threshold value chosen.

Experiments show that when the threshold is large the associated label image is large, resulting in over-segmentation while if the threshold is small the associated label image is small resulting in under-segmentation. Over-segmentation manifests as false positives in the found defect regions, that is regions which are flagged as being defect regions which do not appear to be defect regions. Under-segmentation manifests as false negatives, that is regions which appear to be defect regions but are not so flagged. It is found that for some images both false positives and false negatives are present in the segmentation. Therefore there is no threshold value which results in a completely correct segmentation for all images.

The main segmentation approach that we consider in this paper is based on an adaptation of the segmentation method of the PIRAT system to the case of colour images [9]. The method used in PIRAT is a supervised method which means that the segmentation system is trained by using training examples which are labelled with their correct classifications. For the PIRAT development the training examples were obtained from simulated data while for the proposed system they must be obtained from real data.

The method of segmentation used in the PIRAT system involved feature extraction followed by classification of the feature vector [10]. In the PIRAT project differential geometric features were used and the classifier was the nearest neighbour classifier. Differential geometric features are mainly applicable to range images. Therefore other features have to be used for the colour image segmentation.

A number of authors have used a feature vector consisting simply of the RGB (red, green and blue) values of a pixel as inputs to a classifier [11]. We have also used as a feature set the H, S and B components in the HSB (hue, saturation and brightness) colour space [12].

In addition, a slightly more sophisticated feature set has been implemented in which the max, min and average are computed for RGB values in a window (of size say 7×7) about each pixel together with the max, min and average of an intensity feature I given by

$$\mathrm{I} = \sqrt{\left(\mathrm{R}^2 + \mathrm{G}^2 + \mathrm{B}^2\right)}.$$

Also we have used a more elaborate feature set constructed from Gabor texture filter banks [13]. Gabor filters are useful for analysing the texture properties of images. Gabor filters have been used in many applications including texture segmentation, target detection and image coding. Gabor filters can be described as Gaussian shaped band pass filters. An even-symmetric Gabor filter is obtained by convolving a unit impulse response function of the form

$$\begin{aligned}\mathrm{h}(\mathrm{u},\mathrm{v}) &= \mathrm{h}(\mathrm{u}_0,\theta)(\mathrm{u},\mathrm{v}) = \mathrm{h}(\mathrm{u}_0,\theta,\mathrm{u},\mathrm{v})\\ &= \exp\left\{-(1/2)\left[\mathrm{x}^2/\sigma_\mathrm{x}^2 + \mathrm{y}^2/\sigma_\mathrm{y}^2\right]\right\}\cos(2\pi\mathrm{u}_0\mathrm{x}),\end{aligned}$$

where

$$\begin{aligned}\mathrm{x} &= \mathrm{u}\cos(\theta) - \mathrm{v}\sin(\theta),\\ \mathrm{y} &= \mathrm{u}\sin(\theta) + \mathrm{v}\cos(\theta),\end{aligned}$$

with an input image. The Gabor filter $\Im(\mathrm{u}_0,\theta)$ corresponding to spatial frequency u_0 and orientation θ is given by

$$\begin{aligned}&\Im(\mathrm{u}_0,\theta)\omega = \mathrm{h}(\mathrm{u}_0,\theta)*\omega,\\ &\text{for } \omega : \mathbf{Z}^2 \to [0,\infty),\end{aligned}$$

where

$$(\mathrm{h}(\mathrm{u}_0,\theta)*\omega)(\mathrm{i},\mathrm{j}) = \sum_{k=-\infty}^{\infty}\sum_{l=-\infty}^{\infty}\omega(i-k,j-l)h(u_0,\theta,k,l)\,.$$

Since the mask $\mathrm{h}(\mathrm{u}_0,\theta)$ vanishes exponentially with increasing distance from the origin it can be well approximated by a finite mask. The filter can be considered to act on finite images by null extending finite images to infinite images.

A bank of Gabor filters is obtained by taking a set of values for the radial frequency u_0 and the orientation θ. We have used a set of radial frequencies of the form $\{\sqrt{2}\,2^{-2-\mathrm{i}}: \mathrm{i}=0,1,\ldots,\mathrm{n\_u}_0-1\}$ where $\mathrm{n_u}_0\in\{1, 2, \ldots\}$and a set of orientations of the form $\{0, \pi/4, \pi/2, 3\pi/4\}$ [14]. The above radial frequencies are an octave apart.

For the classifier we used a support vector machine (SVM). SVMs have certain properties that make them superior to neural networks such as requiring smaller training sets and having better generalisation ability.

For generation of a training set for the SVM a set of feature vectors for individual pixels together with their classifications must be extracted from the training data images. The feature vectors can be extracted automatically but the classification labels must be determined manually (if they could be determined automatically then we would have already solved the problem of segmentation).

This manual pixel classification process can be effected by using a GUI program which displays a training image and enables the user to select certain regions or sets of pixels and specify that they are of a particular classification.

A simpler approach to generating training sets for the pixel classifier is to select rectangular regions of constant classification using standard tools. There will be a problem with this method if regions of constant classification do not contain rectangular subsets of a reasonable size.

This simpler approach was used for the experiments of the present paper. Rectangular regions such as those shown in Fig. 3 were selected and extracted from the unwrapped pipe image of a 393 m long concrete sewer pipe (part of which is shown in Fig. 1). The

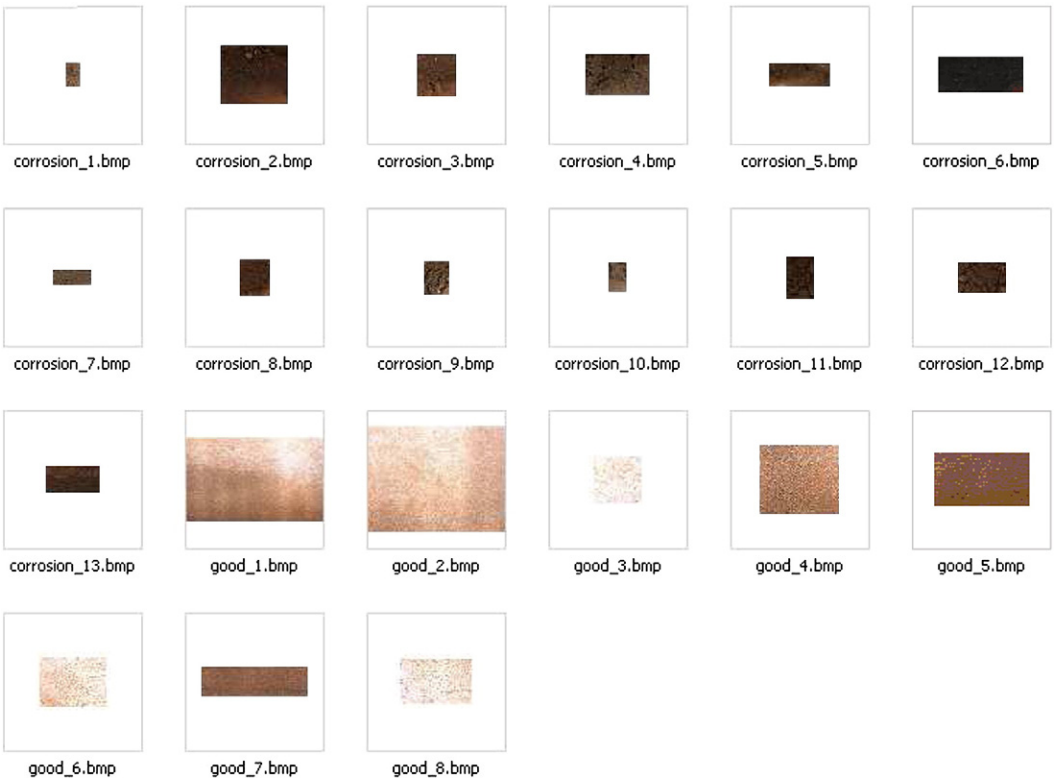

Fig. 3. Rectangular regions of corrosion and good pipe.

regions were extracted from regions of corrosion and regions of good pipe. Two files called good_1.bmp and good_2.bmp were used for testing the classifier while the remaining corrosion and good pipe files were used for both training and testing.

The bitmap files were processed by a program to produce text files containing the RGB values. The RGB values were then processed to produce feature vectors, either RGB, HSB, Gabor or local window features. The files of feature vectors had the classifications (either 0 for good pipe or 1 for corrosion) added in the format suitable for the SVM training program. Training sets and testing sets were then randomly selected from the feature vector files. The data was then rescaled for the purposes of the SVM training so that its minimum and maximum values were 0 and 1 respectively. Then the SVM training was carried out. The results of testing the pixel classifier on the testing sets that had been set aside are shown in Table 1. The table shows that when tested on the testing data that had been set aside during training and on the data contained in good_1.bmp and good_2.bmp the classifier performed well when using all feature sets. In applying the SVM pixel classifiers generally to images other than those used in training blockwise rescaling was applied in order to try to compensate for brightness variations from one part of the pipe image to another.

The SVM pixel classifier algorithms for the RGB, Gabor, local window and HSB feature sets were applied to the image of Fig. 1. The result for the HSB case is shown in Fig. 4. The image labelling results for the RGB and Gabor feature set cases were very similar to but not quite as good as the HSB case. The segmentation in the Gabor case is slightly worse than the segmentation in the RGB case. This is because the pipe joint breaks up to a certain extent with the result that after connected component labelling it would form more than one defect or feature region. Also the algorithm used for the Gabor case requires considerably more processing time than the other algorithms.

Table 1
Classifier test results.

Feature set	No. of training cases	No. of testing cases	% Accuracy of testing	% Accuracy on good_1.bmp	% Accuracy on good_2.bmp
RGB	3000	17,867	96.88	99.15	99.93
HSB	1000	19,867	97.30	99.39	99.98
Gabor	5000	15,867	97.11	99.25	99.92
Window	3999	10,100	99.83	99.98	100.00

The RGB, Gabor and HSB pixel labelling images contain single pixel and other very small defects. These are perhaps not a problem because such defects can be filtered out at a higher level by the pipe inspection system during image classification and analysis.

The local window based pixel classifier image contains regions which are square artefacts of the window method. Also the pipe joint does not extend across the full width of the pipe.

The best result for segmenting the image of Fig. 1 is obtained by using the HSB feature set. Both the pipe joint and the crack on the top left hand side of the image are comparatively strongly demarcated. Similar results have been obtained for other test images from the same 393 m section of sewer under consideration.

4. Detection of corrosion defects and pipe connections

The segmentation operation results in a number of regions for each pipe image. The largest such region which extends over the full length of the pipe is made up from the flow lines at the bottom of the pipe together with any pipe joints radiating out from the flow lines. Also any defective regions which are adjoined to these regions form part of this principal segmented region. Segmented regions other than the principal segmented region form candidates for corrosion regions, other defect regions or pipe connections. In the work of this paper we are concentrating on the defect type of corrosion.

Pipe connections may be distinguished from corrosion regions by using a simple fuzzy approach. A defect region is likely to be a pipe connection if it is located approximately laterally in the pipe and its size is within a range of suitable sizes. One may also consider requiring that its shape as measured by for example a goodness of fit parameter

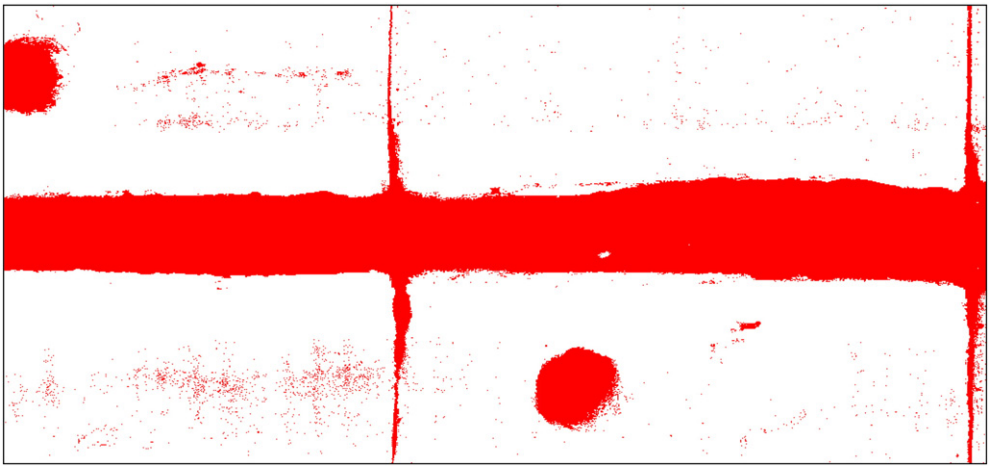

Fig. 4. HSB-SVM pixel labelling.

for an ellipse of best fit is in a suitable range. However, as noted by Müller and Fischer [15] segmented regions arising from pipe connections can come in a number of shapes other than oval.

One may define fuzzy membership functions associated with the conditions that the defect be laterally located and of a suitable size. In line with the usual rule for combining membership functions under conjunction an overall membership function value for whether or not the defect is a pipe connection may be obtained by taking the minimum of these two membership function values. A membership function value for whether the defect is a corrosion may be obtained by taking the complement of the pipe connection membership value. A defect may be declared to be a pipe connection if its pipe connection membership function value exceeds its corrosion membership function value, and a corrosion otherwise. Pipe connection detection by this simple fuzzy approach has been applied to the trial images under consideration with the result of completely accurate detection except in one case where the pipe connection was on the boundary of the image. Cases such as this can be avoided by processing the full unwrapped pipe image or else by using overlapping windows.

Defect regions together with their classification as either corrosion or pipe connection can be displayed by means of a GUI as shown for example in Figs. 5 and 6. The effectiveness of the system at finding defects or features depends upon the quality of the segmentation. For the SVM segmentation the result depends upon the reference brightness parameter used for the blockwise rescaling. When the reference brightness is high the system under-segments resulting in more false negatives. When the reference brightness is low the system over-segments resulting in more false positives. Some values of the reference brightness are associated with both false positives and false negatives. Thus, as in the case of the thresholding method, perfect segmentation cannot be achieved using the SVM method. However, the SVM method has the potential to be a more powerful segmentation method because it takes into account the colour properties of the

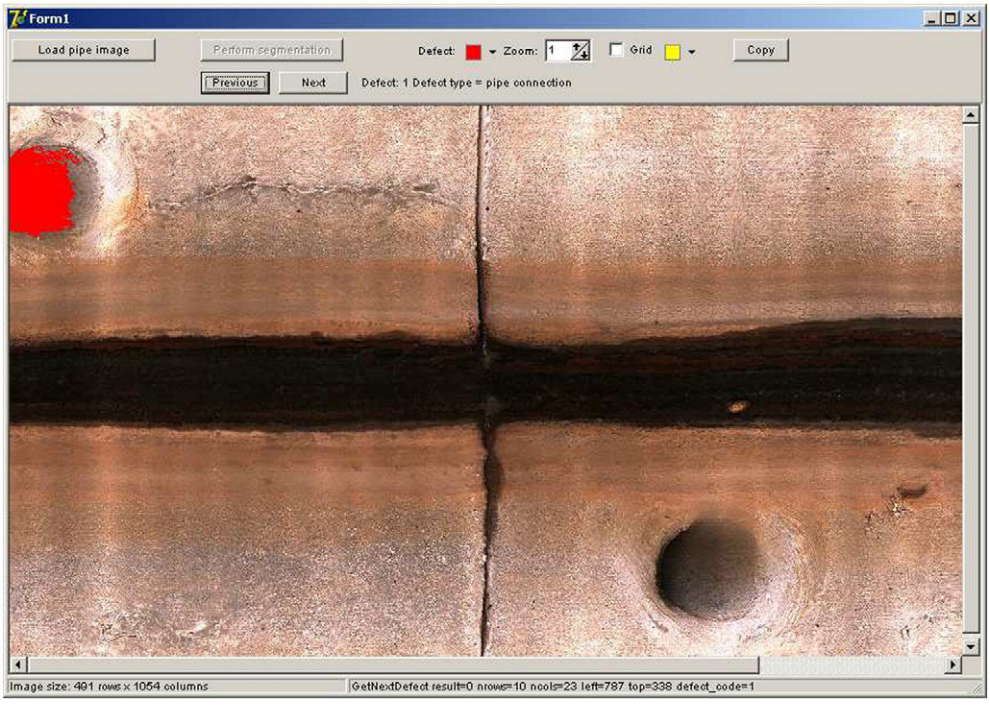

Fig. 5. GUI display of pipe connection.

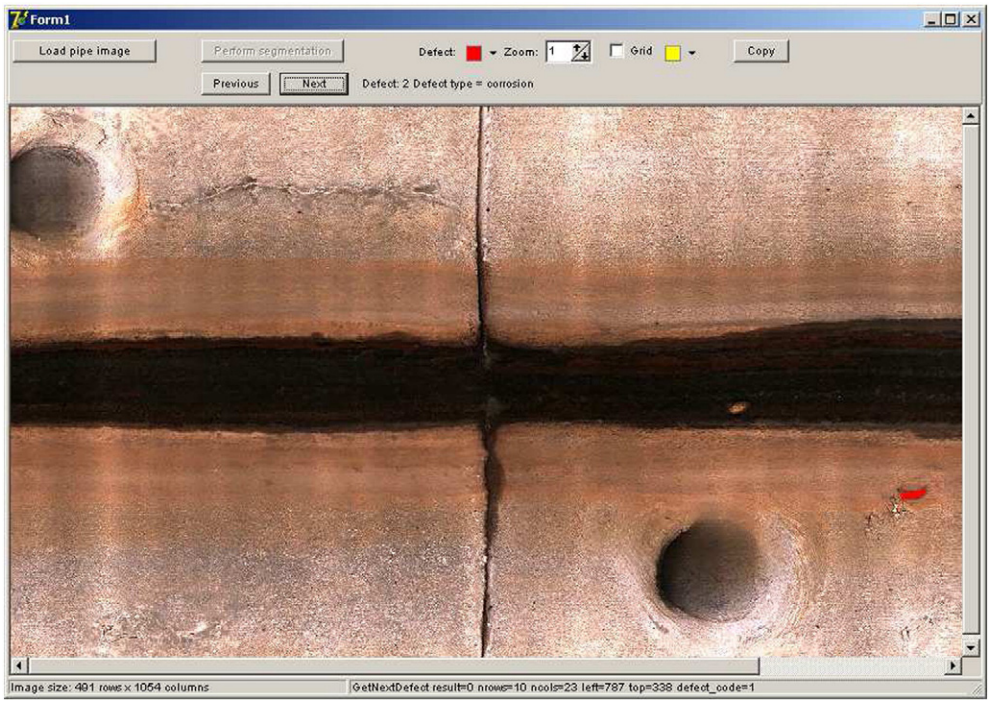

Fig. 6. GUI display of corrosion defect.

images rather than just the grey-scale brightness value and so is utilising more information present in the image.

5. Detection of flow lines, pipe joints and adjoining defects

It is desirable to have a method of decomposing the principal segmented region into its separate parts, that is, flow lines, pipe joints and adjoining defects. This can be achieved using the methods of mathematical morphology.

Grey-scale morphology has been used by Sinha and Fieguth [16] to segment pipe joints and pipe connections. However, in our work, a binary segmented image is already present as a result of prior segmentation using SVM or other method. Therefore the more reliable binary image morphology can be used. Also, we define generalisations of the morphology operations which are more suitable to the images being analysed.

Consider the problem of flow line detection. The image of Fig. 7 is a typical example of a section of pipe containing flow lines, pipe joints and adjoining defects. The result of carrying out binary segmentation by SVM or other method followed by connected component labelling on this image is a collection of connected components. Let Δ_{flow} be an estimate of the width of the flow line region. Define the principal connected component to be the connected component for which the intersection with the band of width Δ_{flow} centred on the bottom of the pipe is the greatest. The principal connected component in this case is shown in Fig. 8. Now we recall that if a binary image is associated with a set $A \subset X$ where $X = \{0,\ldots,m-1\} \times \{0,\ldots,n-1\}$ is the image lattice then the erosion $A \ominus E$ of A with respect to a structuring element $E \subset \mathbf{Z}^2$ is given by

$$A \ominus E = \{x \in X : E_x \cap X \subset A\},$$

and the dilation $A \oplus E$ of A with respect to E is given by

$$A \oplus E = \{x \in X : \hat{E}_x \cap A \neq \emptyset\},$$
$$\text{where } E_x = \{x+e : e \in E\} \subset \mathbf{Z}^2, \hat{E} = \{-e : e \in E\}.$$

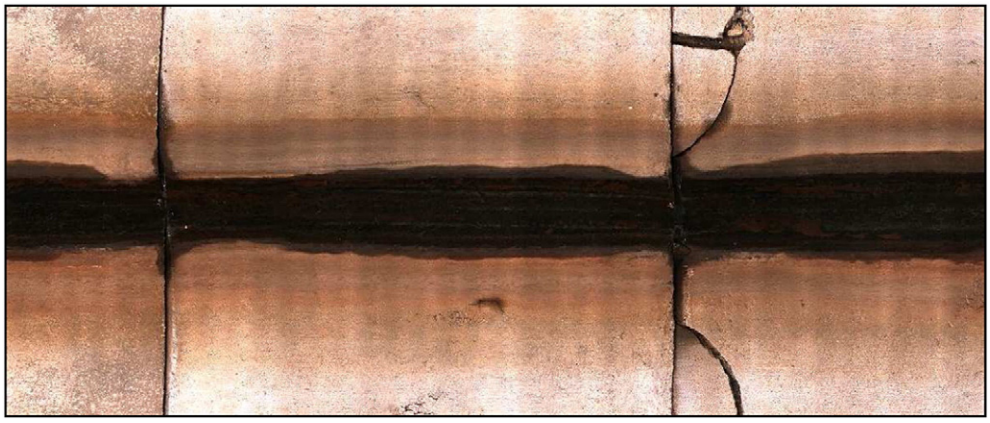

Fig. 7. Typical example of flow lines, pipe joints and adjoining defects.

Fig. 8. Principal connected component.

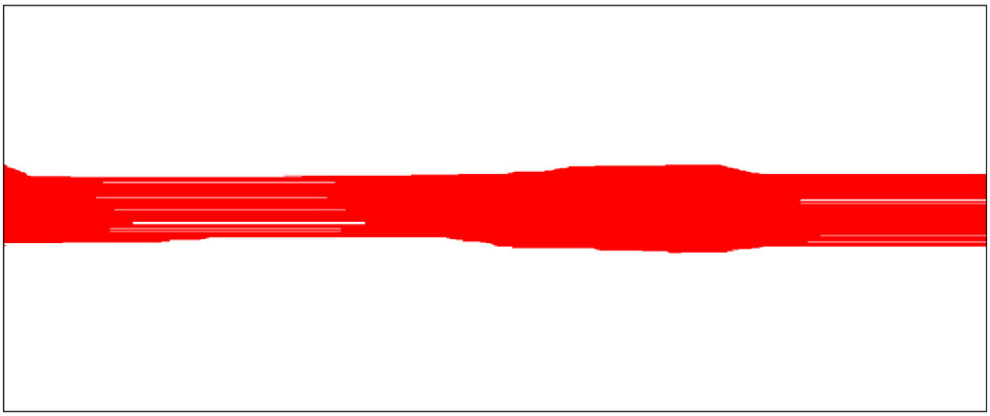

Fig. 9. Erosion of principal connected component.

Let A be the principal connected component shown in Fig. 8. It is natural to try to define the core region of the flow lines to be given by $A \ominus E$ where E is the horizontal structuring element given by

$$E = \{(0, j) : j = -\text{element\_length\_1}, \ldots, \text{element\_length\_1}\}.$$

However, the result of this erosion with element_length_1 = 100 is shown in Fig. 9. The erosion does not provide a good representation of the flow line region. The reason for this behaviour is that some points in the convex hull of the flow line region are missing due to random noise variation. This results in the lines of missing values in the eroded image. This behaviour can be avoided by defining a generalisation of the erosion operation which we will call α-erosion, fractional erosion or partial erosion. Let $\alpha \in [0,1]$. Define the α-erosion $A \ominus_\alpha E$ of A by a structuring element E by

$$A \ominus_\alpha E = \{x \in X : |E_x \cap A| \geq \alpha |E_x \cap X|\},$$

where, for a set S, |S| is the number of elements of S. Thus $A \ominus_\alpha E$ consists of all those points x in X such that the fraction of points in the x-translate of E which are in A is greater than or equal to α.

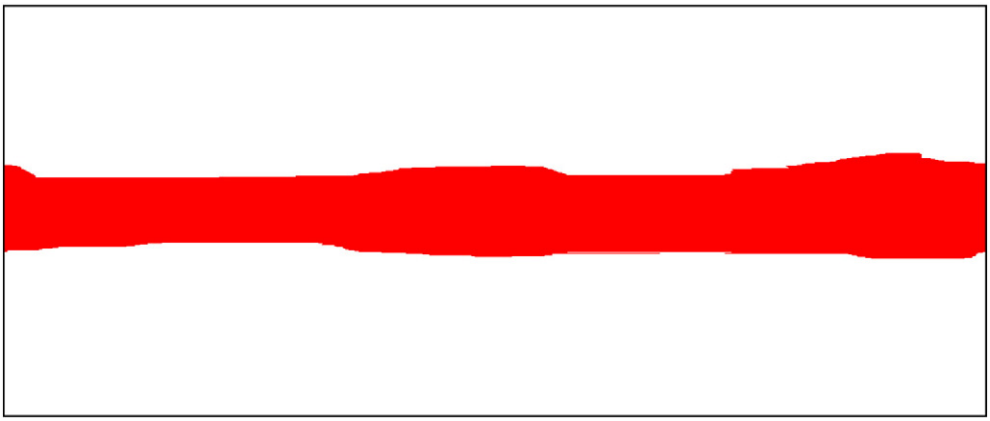

Fig. 10. Core flow line region = α-erosion of principal connected component with $\alpha = 0.9$.

Fig. 11. Principal connected component–core flow line region.

Theorem 1. *For $\alpha = 1$ the α-erosion $\ominus_\alpha$ coincides with the usual erosion $\ominus$.*

A detailed proof of this theorem is given in the Appendix. It is also straightforward to show that

$$\alpha < \beta \Rightarrow A \ominus_\alpha E \supset A \ominus_\beta E,$$

and that

$$A \ominus_0 E = X.$$

We may also define, for $A \subset X$, $E \subset \mathbf{Z}^2$ and $\alpha \in [0,1]$, the α-dilation $A \oplus_\alpha E$ of A by E by

$$A \oplus_\alpha E = \left\{ x \in X : |\hat{E}_x \cap A| > \alpha |E_x \cap X| \right\}.$$

Clearly, for $\alpha = 0$ the α-dilation $\oplus_\alpha$ coincides with the usual dilation $\oplus$, for $\alpha = 1$ $A \oplus_\alpha E = \varnothing$ and $\alpha < \beta \Rightarrow A \oplus_\alpha E \supset A \oplus_\beta E$. Also, we have the following duality theorem connecting $\oplus_\alpha$ and $\ominus_\alpha$.

Theorem 2. $\sim(A \ominus_\alpha E) = \sim A \oplus_{1-\alpha} \hat{E}$.

A detailed proof of this theorem is given in the Appendix. The result of carrying out the α-erosion of the image in Fig. 8 by the horizontal structuring element defined above with element_length_1 = 100 and $\alpha = 0.9$ is shown in Fig. 10. This gives a good representation of the core of the flow line region. The flow line region may be taken to be estimated by the dilation of the core flow line region by the structuring element

$$E = \{(i,0) : i = -\text{element\_length\_2}, \ldots, \text{element\_length\_2}\}.$$

The binary image obtained by taking P ~ F where P is the principal connected component and F is the (estimated) flow line region is shown in Fig. 11. This represents the pipe joints and adjoining defects. Candidate pipe joints may be detected by taking the α-erosion of this image with respect to the structuring element

$$E = \{(i,0) : i = -\text{element\_length\_3}, \ldots, \text{element\_length\_3}\},$$

with the result shown in Fig. 12.

The candidate pipe joint components are the connected components of this image. In the case of the given example, there are 6 such components. Components can be eliminated if the width of the bounding box in the x direction is not sufficiently small. Define the nominal x coordinate of a component to be the x coordinate of the mid point of a horizontal edge of the bounding box of the component. We may define an equivalence relation on the set of components by defining two components to be equivalent if their nominal x coordinates differ by less than a tolerance. The set of components may be grouped into equivalence classes and each such class may be identified with a pipe joint as long as it has components on either side of the flow line region. In the example of Fig. 12 there are two such classes each containing 3 elements and one class not identified with a pipe joint containing 1 element. Elements of the latter type of class may be identified with parts of adjoining defects. We may define the nominal x coordinate of a pipe joint to be the average of the nominal x coordinates of the components that make it up. Finally, we may define the remaining adjoining defect regions to be made up of those points in the image obtained as in Fig. 12 whose x coordinate differs by greater than some tolerance from the nominal x coordinates of all the pipe joints.

The method of pipe joint detection described above has been applied to 23 images of 393 m of concrete pipe under consideration with the result of 100% classification accuracy.

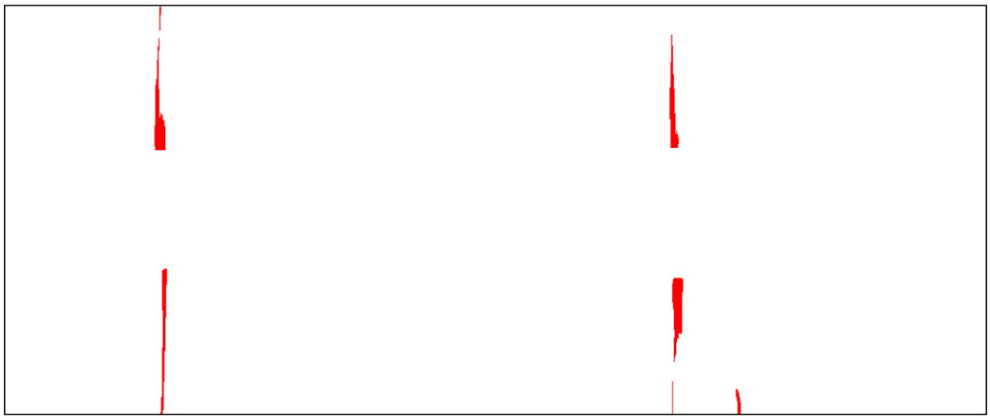

Fig. 12. Candidate pipe joints.

6. Conclusions

An approach to signal interpretation for automatic pipe inspection based on segmentation of colour images by SVM has been presented. The segmentation approach has been tested using RGB, Gabor, local window and HSB feature sets. It has been found that the method works best in the case of the HSB feature set. The segmentation algorithm can be used as part of a pipe inspection system utilising also range image information for the purpose of defect classification. Such range image information can be obtained either directly from the inspection device or else possibly by analysing colour images obtained from the inspection device by photogrammetry. Analysis of the principal connected component of the segmented region by mathematical morphology enables the flow line region, pipe joints and adjoining defects to be detected. While manifesting some false positives or false negatives in corrosion detection, the system had essentially 100% accuracy in the detection of flow line region, pipe joints and pipe connections on the data on which it had been tested.

Acknowledgements

The authors thank Tristan Day for supplying colour images of sewers. Also the authors would like to thank Scott Gould for help with the selection of pipe defect images.

Appendix A. Proof of theorems

Theorem 1. *For $\alpha = 1$ the α-erosion $\ominus_\alpha$ coincides with the usual erosion $\ominus$.*

Proof. We have, for all $x \in X$,

$$x \in A \ominus_\alpha E \Leftrightarrow |E_x \cap A| = |E_x \cap X|.$$

Suppose that $x \in A \ominus E$. Then $E_x \cap X \subset A$. Therefore $E_x \cap A = E_x \cap X$ and so $|E_x \cap A| = |E_x \cap X|$. Thus $x \in A \ominus_\alpha E$. Hence $A \ominus E \subset A \ominus_\alpha E$. Now suppose that $x \in A \ominus_\alpha E$ and suppose, for contradiction, that $x \notin A \ominus E$. Then $E_x \cap X \not\subset A$. Thus $|E_x \cap X| = |E_x \cap A| + |E_x \cap (X \sim A)| > |E_x \cap A|$ which contradicts the fact that $x \in A \ominus_\alpha E$. Thus $x \in A \ominus E$. Hence $A \ominus_\alpha E \subset A \ominus E$. It follows that $A \ominus_\alpha E = A \ominus E$.

QED

Theorem. *$2 \sim (A \ominus_\alpha E) = \sim A \oplus_{1-\alpha} \hat{E}$.*

Proof. For all $x \in X$

$$\begin{aligned} x \in \sim(A \Theta_\alpha E) &\Leftrightarrow x \notin A \Theta_\alpha E \\ &\Leftrightarrow |E_x \cap A| < \alpha |E_x \cap X| \\ &\Leftrightarrow |E_x \cap X| = |E_x \cap A| + |E_x \cap (X \sim A)| < \alpha |E_x \cap X| + |E_x \cap (X \sim A)| \\ &\Leftrightarrow |E_x \cap (X \sim A)| > (1-\alpha) |E_x \cap X| \\ &\Leftrightarrow x \in \sim A \oplus_{1-\alpha} \hat{E}. \end{aligned}$$

QED

References

[1] H. Kuntze, H. Haffner, M. Selig, D. Schmidt, K. Janotta, M. Loh, Development of a flexible utilisable robot for intelligent sensor-based sewer inspection, Proc. of the 4th International Conference on Pipeline Construction, Hamburg, Germany, 1994, pp. 367–374.
[2] R. Kirkham, P.D. Kearney, K.J. Rogers, J. Mashford, PIRAT — a system for quantitative sewer pipe assessment, The International Journal of Robotics Research 19 (11) (2000) 1033–1053.
[3] J.S. Mashford, A neural network image classification system for automatic inspection, Proc. of the 1995 IEEE International Conference on Neural Networks, Perth, Australia, 1995, pp. 713–717.
[4] O. Moselhi, Shehab-Eldeen, Classification of defects in sewer pipes using neural networks, Journal of Infrastructure Systems 6 (3) (2000) 97–104.
[5] S.K. Sinha, F. Karray, Classification of underground pipe scanned images using feature extraction and neuro-fuzzy algorithm, IEEE Transactions on Neural Networks 13 (2) (2002) 393–401.
[6] O. Duran, K. Althoefer, L.D. Seneviratne, Automated pipe defect detection and categorization using camera/laser-based profiler and artificial neural network, IEEE Transactions on Automation Science and Engineering 4 (1) (2007) 118–126.
[7] H.D. Cheng, X.H. Jiang, Y. Sun, J. Wang, Color image segmentation: advances and prospects, Pattern Recognition 34 (2001) 2259–2281.
[8] O. Moselhi, T. Shehab-Eldeen, Automated detection of surface defects in water and sewer pipes, Automation in Construction 8 (1999) 581–588.
[9] J. Mashford, P. Davis, M. Rahilly, Pixel-based colour image segmentation using support vector machine for automatic pipe inspection, Lecture Notes in Artificial Intelligence, 4830, Springer-Verlag, Berlin, 2007, pp. 739–743.
[10] W.E. Blanz, S.L. Gish, A real-time image segmentation system using a connectionist classifier architecture, International Journal of Pattern Recognition and Artificial Intelligence 5 (4) (1991) 603–617.
[11] H. Gomez-Moreno, P. Gil-Jimenez, S. Lafuente-Arroyo, R. Vicen-Bueno, R. Sanchez-Montero, Color image segmentation using the support vector machines, Recent Advances in Intelligent Systems and Signal Processing, 2003, pp. 151–155.
[12] R. Gonzalez, R. Woods, Digital Image Processing, 2nd ed, Prentice Hall Press, 2002, p. 295.
[13] S.E. Grigorescu, N. Petkov, P. Kruizinga, Comparison of texture features based on Gabor filters, IEEE Transactions on Image Processing 11 (10) (2002) 1160–1167.
[14] T. Randen, J.H. Husøy, Filtering for texture classification: a comparative study, IEEE Transactions on Pattern Analysis and Machine Intelligence 21 (4) (1999) 291–310.
[15] K. Müller, B. Fischer, Objective condition assessment of sewer systems, Proc. LESAM 2007—2nd Leading Edge Conference on Strategic Assessment Management, Lisbon, Portugal, 2007, pp. 1–13.
[16] S.K. Sinha, P.W. Fieguth, Segmentation of buried concrete pipe images, Automation in Construction 15 (2006) 47–57.